ELSEVIER

Journal of Nuclear Materials 274 (1999) 23–33

journal of nuclear materials

www.elsevier.nl/locate/jnucmat

Preliminary fabrication and characterisation of inert matrix and thoria fuels for plutonium disposition in light water reactors

F. Vettraino [a,*], G. Magnani [b], T. La Torretta [b], E. Marmo [d], S. Coelli [e], L. Luzzi [e], P. Ossi [e], G. Zappa [c]

[a] *ENEA-Nuclear Fission Division, Via Martiri di Monte Sole 4, 40129 Bologna, Italy*
[b] *ENEA-INN/NUMA, Faenza Research Center, 48018 Faenza, Italy*
[c] *ENEA-INN-NUMA, Casaccia Research Center, 00060 Rome, Italy*
[d] *FN-New Technologies and Advanced Services, 15062 Bosco Marengo, AL, Italy*
[e] *Polytechnic of Milan, Department of Nuclear Engineering, Via Ponzio 34/3, 20133 Milan, Italy*

Abstract

The plutonium disposition is presently acknowledged as a most urgent issue at the world level. Inert matrix and thoria fuel concepts for Pu burning in LWRs show good potential in providing effective and ultimate solutions to this issue. In non-fertile (U-free) inert matrix fuel, plutonium oxide is diluted within inert oxides such as stabilised ZrO_2, Al_2O_3, MgO or $MgAl_2O_4$. Thoria addition, which helps improve neutronic characteristics of inert fuels, appears as a promising variant of U-free fuel. In the context of an R&D activity aimed at assessing the feasibility of the fuel concept above, simulated fuel pellets have been produced both from dry-powder metallurgy and the sol–gel route. Results show that they can be fabricated by matching basic nuclear grade specifications such as the required geometry, density and microstructure. Some characterisation testing dealing with thermo-physical properties, ion irradiation damage and solubility also have been started. Results from thermo-physical measurements at room temperature have been achieved. A main feature stemming from solubility testing outcomes is a very high chemical stability which should render the fuel strongly diversion resistant and suitable for direct final disposal in deep geological repository (once-through solution).

1. Introduction

The reference background is about 100 t of excess plutonium (WG-Pu) that are originated from warhead dismantling under the START I and II agreements and approximately another 200 t of civilian or reactor-grade Pu (RG-Pu) already stockpiled from commercial spent fuel reprocessing. Total RG-Pu generated is forecasted to reach some 1200 t by the year 2000.

Three generic fuel types are possible to burn plutonium in LWRs [2,3]: uranium-based mixed oxides $(U,Pu)O_2$ also called MOX fuel; thorium-based mixed oxides $(Th,Pu)O_2$ and inert matrix fuels (IMF), where PuO_2 is dispersed in a neutron transparent ceramic carrier.

Civilian mixed-oxide $(U,Pu)O_2$ fuels [4,5] have been thoroughly studied and tested, and wide operational experience is now available on a commercial basis. In fact they have been indicated by both US and Russia as the reference option for the in-reactor disposition of their WG-Pu. Their main drawback, however, is the new plutonium which is continuously generated during irradiation, so that a significant fraction (~70%) of the loaded plutonium is still present in the discharged spent fuel, although it is denatured.

The $(Th,Pu)O_2$ fuel creates interest because of its potential for increasing the Pu consumption with respect to $(U,Pu)O_2$, due to the lack of U. Moreover, there exist experimental data on thoria fuels, that indicate a good under irradiation behaviour and a rather high stability

* Corresponding author. Fax: +39-051 6098 688; e-mail: vett@bologna.enea.it

0022-3115/99/$ – see front matter
PII: S0022-3115(99)00039-2

for the resulting spent fuel, so that it is likely to be appropriate for direct disposal. A major disadvantage for Th-fuel is the ^{233}U breeding, though the high gamma activity of the separated uranium mixture, coming mainly from ^{232}U, should highly discourage this possible proliferation pathway.

The primary advantage of U-free inert matrix fuel [2,3,6,7] is the non-production of new plutonium during irradiation, due to lack of uranium (U-free fuel) whose ^{238}U isotope is the departure nuclide for breeding ^{239}Pu. In addition it enables nearly total destruction of fissile Pu (inherent non-proliferant fuel).

In the inert matrix and thoria fuel concept plutonium oxide is diluted in inert ceramic oxides (e.g. stabilised zirconia or spinel) and/or thoria, in such a content as to give approximately the same reactivity performances as in the standard ^{235}U enriched fuel for LWRs.

To cope with low thermal conductivity or low melting point, annular pellets are foreseen for zirconia and spinel use. Burnable poisons also have to be envisaged for controlling peaking factors and burn-up reactivity swings. A major drawback for U-free IMF remains however the low Doppler coefficient as a consequence of lack of ^{238}U.

ThO_2 is considered mainly to improve reactivity feedbacks (Doppler) in pure inert matrix fuel, strenghten chemical stability and accelerate Pu stock disposition. A partial introduction of ThO_2 in the matrix (thoria-doped fuel) or total (thoria–plutonia fuel) is possible [1–3]. To cope with the problems arising from the proliferation standpoint when using thoria (^{233}U breeding from ^{232}Th), it is possible to add some limited amount of depleted U in order to denature the produced ^{233}U. Moreover, the thoria introduction is also applicable to the Pu–Th cycle as forecasted in a hybrid accelerator driven system (ADS) envisaged to act as a burner machine either for plutonium or minor actimides and long-lived radwastes [8,9]. In this latter context Th utilisation could constitute an additional option, further of the solution here proposed, which would permit the ^{233}U recoverability under suitable anti-proliferation countermeasures.

The explored pellet fabrication processes are the sol–gel, gel supported precipitation (GSP) and mixed powders route. The GSP process would provide the advantage of free-flowing, dust free, highly homogeneous microspheres with enhanced characteristics of sinterability. The standard LWR geometry is the reference one for: pellet, pin and fuel assembly.

Finally, an R&D effort on innovative U-free fuels such as the inert matrix non-proliferant fuel, appears widely justifiable also by the fact that for WG-Pu transmutation in LWRs, the precisely required MOX fuel is not readily available while processes and facilities have to be set-up before reaching the operational stage.

This paper complements the other one provided by Lombardi et al. [10].

2. Preliminary fabrication and characterisation testing

A co-operative R&D activity aimed at assessing the experimental response has been jointly undertaken by ENEA and Polytechnic of Milano, starting from fabrication-characterisation tests on simulated cold material, with the aim of fabricating and irradiating a small lot of Pu-bearing inert matrix fuel with thoria additions.

Some simulated-fuel fabrication and characterisation tests have been carried out on stabilised zirconia, spinel and a mixed matrix alumina–zirconia–magnesia. In this study, however, the plutonium oxide is simulated by cerium oxide (CeO_2). Both processes, the sol–gel GSP and dry powder metallurgy, are investigated for a direct comparison. The objective of fabrication and characterisation tests on cold materials is to demonstrate the capability of producing sintered pellets which comply with basic requirements descending from standard UO_2 and MOX fuels [11], such as: pellet geometry of 8.2 mm diameter and 10.4 mm height; pellet density is approximately 95% TD; maintaining the required porosity in the ceramic material; single crystalline phase and microstructure having an average grain size in the range 10–40 μm; appropriate basic thermo-physical and chemical properties.

2.1. Simulate fuel fabrication tests on Al_2O_3–MgO–ZrO_2 matrix

2.1.1. Experimental procedure

Simulated fuel microspheres have been produced via the GSP process as described in [12,13] starting from a Zr, Mg, Al, Ce nitrate salts and yttria solution. As reported in Fig. 1, to obtain simulated fuel powders we started from microsphere dried in air which was followed by a grinding step. The used composition of simulated fuel (microspheres or powder) was: Al_2O_3 47.8 mol%, ZrO_2 (stabilised with Y_2O_3 16 wt%) 42.4 mol%, MgO 4.9 mol%, CeO_2 (plutonium oxide simulator) 4.9 mol%.

Forming and sintering behaviour was studied by means of manufacturing several samples at different forming pressure within the range 35–500 MPa. Green specimens were sintered in air at 1823 K for 2 h. Sintering cycle had heating and cooling phases at a rate of 300 K h^{-1}.

For all cases, the bulk density of uncompacted sintered microgranules or powders, determined by using the helium pycnometer (Accupyc 1330-Micromeritics) method, was assumed to be the theoretical density (TD) of the simulated fuel. Densities of green and sintered

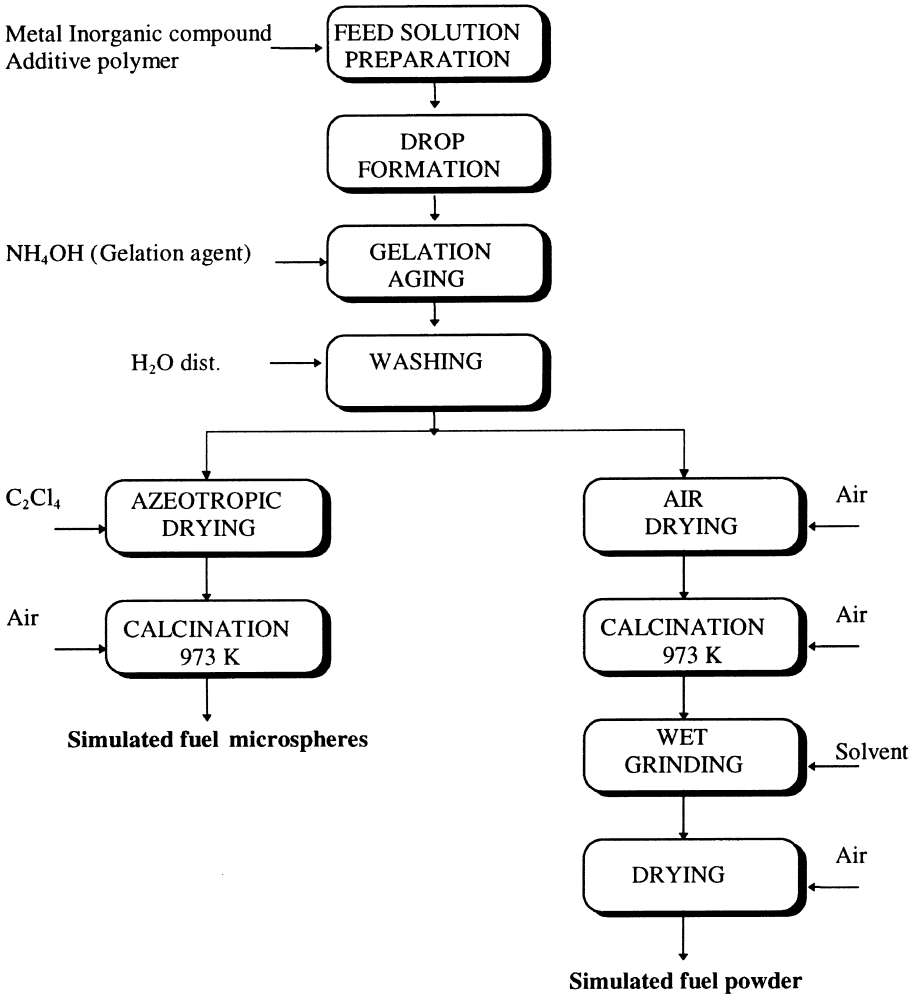

Fig. 1. GSP process flowsheet.

samples were determined by means of volume and weight determination. Crystalline phase identification of sintered pellets was performed by an X-ray diffraction technique (Rigaku–Miniflex, CuKα 1.54 Å). Microsphere shape, powder morphology and sintered sample microstructure were examined by SEM (Stereoscan 250 – Cambridge).

2.1.2. Results and discussion

In the SEM micrograph reported in Fig. 2(a) the typical spherical shape of a simulated fuel microsphere is shown. Microspheres average 100–150 μm in size. Microsphere size was dependent on feed solution flow rate, design of atomizer device and rotation speed. As reported in Ref. [1], microspheres produced by the GSP process had spherical shape due to the water soluble polymeric compound addition which causes a viscosity increasing of the solution used. An SEM micrograph of the powder is reported in Fig. 2(b).

Forming and sintering behaviour was studied with the aim of producing sintered samples with relative density of 95–96% TD. Compaction response of green pellets formed at different pressures is reported in Fig. 3(a). In these curves it is recognisable that breakpoint pressure is in agreement with the compaction response diagram elaborated by Van Der Graaf et al. [14]. In Fig. 3(b), sintering density as a function of forming pressure is shown. The obtained sintered pellet density is 96% TD, reached at pressure of 250 and 150 MPa for microspheres and powders, respectively (theoretical density, as defined above, is 4.90 ± 0.01 g cm^{-3}). Finally, XRD analysis was performed to define crystallographic composition of the sintered pellets. Fully stabilised zirconia was found to be the main phase; other

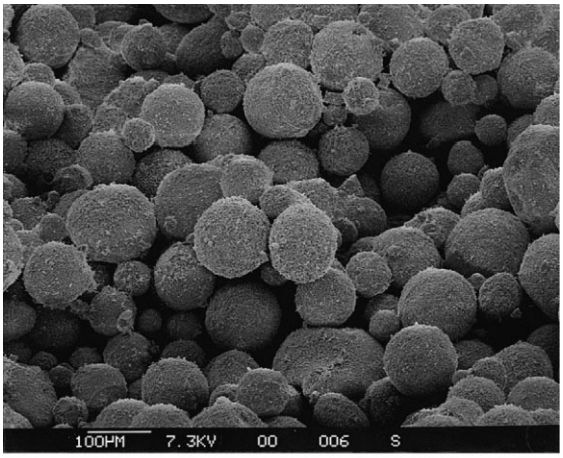

(a)

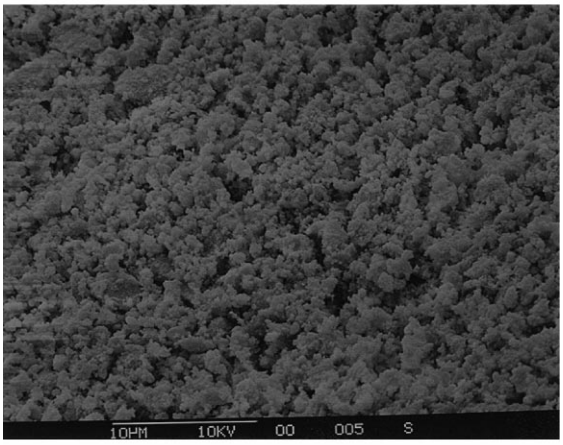

(b)

Fig. 2. SEM micrograph of calcinated material: (a) microspheres; (b) powder.

phases were alumina, magnesium aluminate (spinel) and $MgAl_{11}CeO_{19}$.

2.2. Simulate fuel fabrication tests on stabilised ZrO_2 and spinel matrices

2.2.1. Experimental procedure

The used material compositions were (ZrO_2–19.57%CaO, mol%) and $MgAl_2O_4$ as inert matrices; (ZrO_2–18.2%CaO–7%CeO_2, mol%) and ($MgAl_2O_4$–7%CeO_2, mol%) as simulated fuel.

Powders and microspheres were prepared by coprecipitation and the GSP sol–gel route, respectively.

In the coprecipitation method used for powders' preparation, the departure nitrate salts of Zr, Ca, Mg, Al and Ce are dissolved in water, and then ammonia is added to the colourless solution till an alkaline pH is achieved (pH > 11). In this way, an insoluble salt is precipitated from the solution, filtered onto paper filters and put in a crucible. After moisture elimination, the precipitate is calcinated up to 1073 K for 2 h and the resulting powders are then milled for the required time.

In the sol–gel route (GSP), the solution is also prepared from the water soluble salts of metals as above. Water is added until the solution reaches 80–160 g l^{-1} in total oxide concentration. The solution is then thickened by an organic water soluble polymer, and dropped in a dilute ammonia solution. A surfactant in the ammonia solution ensures the drops do not stick to each other and precipitate to the bottom.

The spheres are removed from the ammonia solution and dried by azeotropic distillation.

Chlorinated hydrocarbon was used as the solvent. The spheres were calcinated in muffle up to 1073 K for 2 h.

At this stage, powders and microspheres were analysed by SEM and XRD to obtain the morphology of

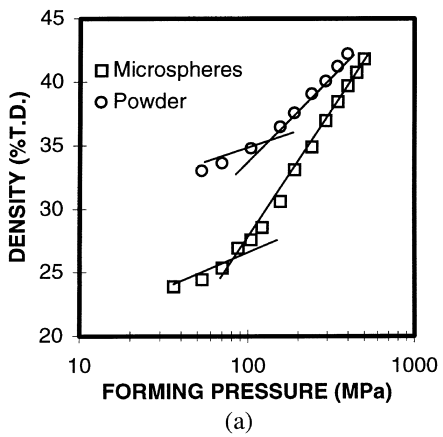

(a)

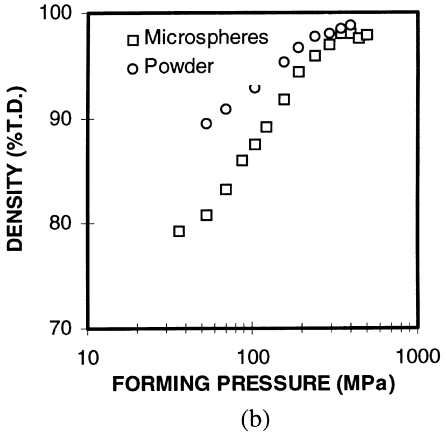

(b)

Fig. 3. Pellet density diagram: (a) green pellet; (b) sintered pellet.

the particles and crystallite phase and size. Specific surface area (BET), density using helium pycnometry and granulometry were also measured.

Green pellets were produced by uniaxial pressing of ceramic powders or microspheres, in a 13.26 mm diameter die with added lubricant. Different forming pressures within the range 100–1000 MPa were applied to evaluate the response of the materials. Green pellets were sintered in an air furnace. The thermal cycles were: 1793 K for 4 h; 1843 K for 2, 4 and 6 h; 1873 K for 2 h, to study grain growth evolution with heating rate of 100 K h^{-1}.

Geometrical density of sintered samples was measured. Bulk density was determined for the best (most dense) pellets by He and Hg pycnometry. Determination of porosity was made by water immersion. Microstructure and phase analysis was performed by SEM (with EDS microanalysis) and XRD techniques.

2.2.2. Results and discussion

For each material composition and production process the main characteristics of powders or microspheres and of sintered pellets are listed in Table 1.

GSP with azeotropic dehydration of gel microspheres (applied for zirconia based materials) permitted us to obtain the required pellet densification, at a sintering temperature of 1843 K. In all other processes, based on powder preparation by coprecipitation and drying in air, lower densities were achieved (from 80 to 94% TD). Different thermal treatments or higher sintering temperature and time may be necessary to meet specifications in this case. Probably extensive milling to sub-micron particle dimensions should give more reactive powders (to be reagglomerated for pressing) though such a step is undesirable with plutonium-containing powders. The coprecipitation of all components gave results very similar to those obtained from mechanical mixing of separated powders (CeO_2 added to inert matrix); this process, preliminary to the GSP one, is not taken into consideration for future developments, but permits us to dissolve a Pu simulator in solid solution with a matrix. With the GSP process, phase and microstructure are completely satisfactory: only cubic-stabilised zirconia is present. In the calcia-stabilised zirconia pellets, a tendency of Ca to segregate at grain boundaries was noted. Average grain size easily reaches minimum requested dimension (10 μm); prolonging sintering time grains grows up to 40 μm. Coprecipitated powders did not show such good behaviour and the large porosity causes inhomogeneity at the microscopic level, inhibiting grain growth and giving a less significative grain size measure. The effect of incrementing the forming pressure is an increase in green body density, giving dense sintered pellets only up to an optimal pressure limit. Once exceeding this limit, lamination and density inhomogeneities are produced. The use of binders and lubricants improves the pressing behaviour; in our case less pressure was needed to obtain higher densities and more regular geometry (squareness and smoothness) with binder addition was achieved. Temperature rise was properly modified in order to permit binder elimination.

A further remark on the GSP method is that it provides a better flow for the press feed and improved capability for automatisation and remotisation of operations in view of Pu-bearing fuel. Moreover, it holds the advantage of avoiding fine contamination when Pu will be present and guarantees homogeneity in the microsphere solid solution, by making sintering easier at lower temperatures.

However, in view of plutonium-based fuel fabrication, attention to the aspects dealing with criticality risk and contaminated effluents coming from the process will be necessary.

Pellet microstructures related to calcia-stabilised zirconia, after thermal eatching, are shown in Fig. 4(a) and (b).

3. Specific characterisation

The following tests are performed on sintered pellets in order to achieve a basic characterisation picture, before starting fabrication on real fissile-bearing fuel:

- Measurement of thermo-physical properties such as: thermal conductivity, specific heat, thermal expansion, melting point and molten material behaviour.
- Solubility tests (corrosion and dissolution). Different conditions are simulated: long-term geological disposal (about room T, pH $\sim$ 8); fresh-spent fuel reprocessing (HNO_3 – 8M, 393 K); PWR operation (573 K, 15.5 MPa, pH 7.2).
- Ion irradiation damage (IID) testing: exploration on targets by using accelerated 180 keV ions (He, Xe), for different ion doses in the range 10^{14}–10^{17} ions cm^{-2}.

Results are given hereafter only on the first two points, owing to the IID testing still being underway.

3.1. Thermophysical properties

A measuring technique [15,16] – based on the thermoelastic effect [17–19] – has been recently developed and qualified at the Department of Nuclear Engineering of Politecnico of Milano, allowing the simultaneous determination of the following thermophysical properties: diffusivity a, conductivity κ, linear expansion coefficient α and specific heat c_p. Moreover, as the experimental apparatus exploits a conventional material testing machine, some additional indications about the mechanical behaviour of tested materials can be easily obtained.

Table 1
Calcia-stabilized zirconia and spinel testing

Material composition	Production process and sintering cycles	Powders and microspheres			Sintered pellets				
		ρHe (g cm^{-3})	BET (m^2 g^{-1})	Optical pressure (MPa)	ρHg (g cm^{-3})	ρHe (g cm^{-3})	Open pore (% vol)	Crystalline phase	Microstructure morphology and average grain size
ZrO_2 + Cao (9.97 wt%) (TD = 5.71 g cm^{-3})	GSP + azeotropic dehydration of microspheres 1793 K, 4 h 1843 K, 4 h	5.07	44.4	600	5.39 (95)	5.41	1	Cubic only	Uniform 15 μm (1793 K, 4h) 30 μm (1843 K, 4h)
	GSP + essication in air of microspheres 1843 K, 2–4–6 h	5.14	16.2	500	4.52 (79)	5.50	18	Cublic only	Not uniform 16 μm (1843 K, 6h)
	Copr. powders 1843 K, 4 h	4.95	30.9	500	4.55 (80)	5.47	17	Not fully stabilized (cub + mon)	Not uniform Grains not visible
ZrO_2 + CaO (8.92 wt%) + CeO_2 (10.53 wt%) (TD = 5.84 g cm^{-3})	GSP + azeotropic dehydration of microspheres 1843 K, 2–4–6 h	5.37	41.4	530	5.61 (96)	5.63	0.4	Cubic only	Uniform 18 μm (1843 K, 2h) 40 μm (1843 K, 6h)
	Mixed powders 1843 K, 4 h	5.15	25.3	750	4.96 (85)	5.56	11	Not fully stabilized (cub + mon)	Not uniform Grains not visible
$MgAl_2O_4$ (TD = 3.76 g cm^{-3})	Copr. powders 1843 K, 4 h	3.28	62.1	450	3.23 (90)	3.49	7.5	Spinel phase	Uniform 2 μm (1843 K, 4h)
$MgAl_2O_4$ + CeO_2 (8.35 wt%) (TD = 3.76 g cm^{-3})	Mixed powders 1843 K, 4 h	3.41	61.2	450	3.53 (94)	3.65	4	Spinel phase + MgO + CeO_2	Not uniform Grains not visible

ρHe = helium pycnometry density; ρHg = mercury pycnometry density with %TD in parentheses; BET = specific surface area; copr. for coprecipitation; cub + mon for cubic + monocline; $TD = 1/\Sigma_i$ ($\%wt_i/\rho_i$), where ρ_i and $\%wt_i$ are, respectively, the theoretical density and the weight percent fraction of the ith component in the mixed compound.

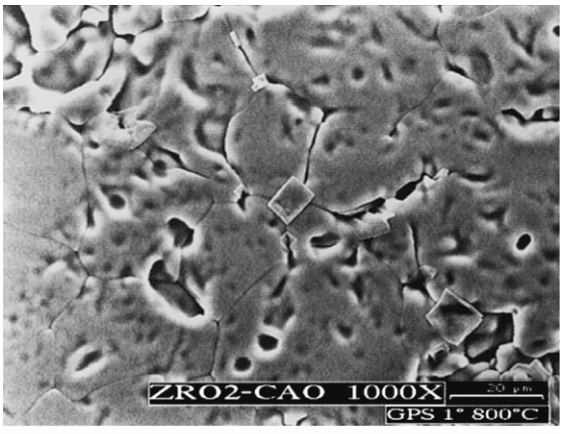

Fig. 4. Sintered pellet microstructure (from sol–gel route): (a) ZrO_2–CaO; (b) ZrO_2–CaO–CeO_2.

A homogeneous heat source is produced for a time t_0 in a cylindrical sample by a uniaxial and uniform compression, well within the linear elastic range of the specimen. The heating process is followed by a thermal relaxation phase at constant stress and null effective thermoelastic source. Under appropriate conditions, the resulting temperature variation ΔT during the thermal relaxation has the simple exponential time dependence

$$\Delta T = \Delta T_{\max} e^{-(t-t_0)/\tau}. \quad (1)$$

The characteristic heat diffusion time τ of the sample and the maximum temperature variation $\Delta T_{\max}$ (typically of the order of 0.1 K) are therefore accessible by a fit of the measured thermal evolution to the form (1); from the obtained values of τ and $\Delta T_{\max}$ the thermal diffusivity a and the ratio α/c_p can be directly derived [20].

The experimental set-up is described elsewhere in detail [21]; here a schematic drawing is shown together with a typical temperature transient during the test (Fig. 5). Theoretical analysis and extensive experimentation allowed us to optimise specimen preparation (geometry, size, surface finishing) and to identify the testing procedures under which the thermoelastic method leads to reproducible and precise results for a large class of elastic materials. The various factors relevant for the measured thermal transients were analysed and criteria for data analysis were accordingly developed [21,22]. The technique has been finally calibrated by reference materials, including certified reference materials (CRM) for thermal conductivity, thermal expansion and specific heat [23,24], resulting in precise assessments for the uncertainty (below 3%) and the accuracy (better than 10%) of measurements.

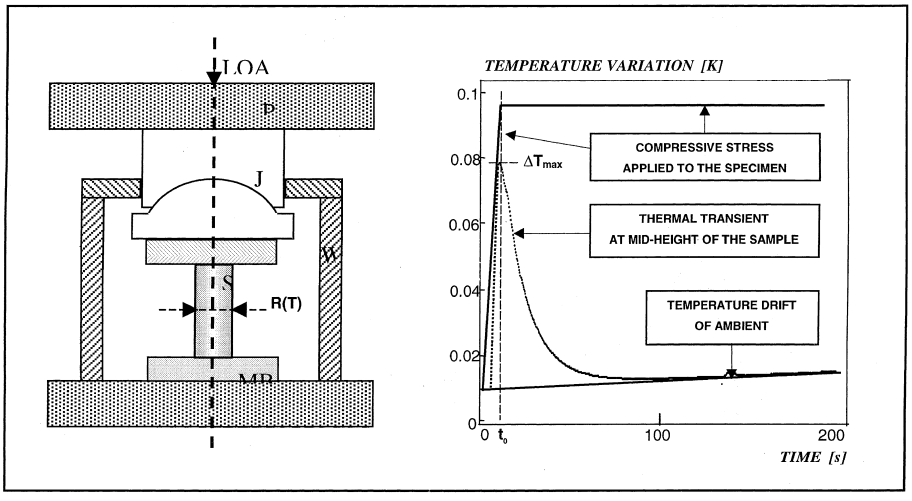

Fig. 5. The employed experimental set-up with a typical temperature transient during the test (P: compression plate; J: ball-and-socket joint; S: specimen; R(T): temperature sensor; MB: molybdenum-bearing block; W: thermoinsulating wall).

Preliminary results at room temperature for several ceramic specimens prepared by FN-New Technologies (see Section 2.2) are shown in Table 2; the thermal conductivity ($\kappa = a \cdot \rho \cdot c_p$) and the linear expansion coefficient α are derived from direct experimental results (i.e. τ and ΔT_{max}) exploiting the reported values of mass density ρ (Archimede's method) and specific heat c_p measured by differential scanning calorimetry (DSC). Due to the thermal conductivity trend of zirconia (rather constant up to temperature of around 1500 K), the κ values found here are also significant for a field of much higher temperatures [7,20]. Work is in progress to perform measurements at higher temperatures.

3.2. Solubility tests

Leaching and dissolution tests were carried out in order to assess the material behaviour under simulation conditions of long-term geological disposal (leaching in ground water) and fresh-spent fuel reprocessing (HNO_3 – 8M, 393 K), including even more aggressive conditions such as chemical attack by HNO_3 (1 ml) + HF (4 ml) concentrated solution at elevated temperature.

3.2.1. Experimental

The different types of tests performed on different materials are reported in Table 3. Two types of matrices were tested: ZrO_2–8.4%$YO_{1.5}$–45.4%Al_2O_3–1.9%MgO (wt%), matrix type A and the ZrO_2–9.7%CaO (wt%), matrix type B. Tests were performed either on pure inert matrix or simulated fuel (inert matrix added with CeO_2). The samples were analysed in different forms: microgranules calcinated at 973 K, sintered at 1823 K, whole sintered pellets and pulverised pellets. The size of the samples was approximately 2.5 g in the case of matrix type A and 5 g in the case of matrix type B or equivalent weight for microgranules or powder samples. In the case of extremely aggressive treatment with concentrated HNO_3 + HF, a very small size sample of 200 mg was employed.

Simulated rain water was used for the leaching tests, prepared according to composition of NIST SRM 2694-II standard. The simulated ground water was obtained by raising to 8.0 the pH of this solution by Na_2CO_3 addition.

Sequential tests at high pressure and temperature in a microwave reactor were carried out for more severe leaching tests (pH = 3.6) and for HNO_3 – 8M dissolution tests.

All the resulting solutions were analysed for the concentration of matrix elements (Zr, Y, Al, Mg and Ce in the case of matrix A and Zr, Ca and Ce in the case of matrix B) by means of the inductively coupled plasma-atomic emission spectroscopy (ICP-AES) technique. The amount of solubilised substances was calculated as a sum of the corresponding oxides of the elements measured in solution. The results are gathered in Table 3 in terms of weight%.

3.2.2. Results and discussion

The results reported in Table 3 show that the investigated materials are particularly dissolution resistant.

Leaching tests on sintered material revealed that in all cases (including very aggressive conditions such as pH = 3.6, $P = 2.5$ MPa, $T = 493$ K) only a few μg (<0.005% total sample weight) of some elements are released in solution. Considering that in all the leaching tests performed, Zr was never detectable in solution and that in the leaching test at pH 8.00 the only element detected in solution was Mg, it is plausible that elements solubilised in the leaching tests were impurity traces containing matrix elements in different chemical forms (e.g. trace of residual reagents or intermediate, trace of soluble compounds formed by reaction with other unknown elements). This hypothesis is supported by results obtained in the sequential test in which it is evident that after the 'cleaning' of the material no matrix elements are released in the solution in the same conditions.

Also in the case of HNO_3 treatment it seems reasonable to draw the same conclusions, though the results

Table 2
Thermophysical data for tested materials (room temperature)

Material Production process	ρ (g cm^{-3})	ρ (% TD)	c_p (J kg^{-1} K^{-1})	a (10^{-7} m^2 s^{-1})	κ (W m^{-1} K^{-1})	α (10^{-6} K^{-1})
ZrO_2 + Cao						
GSP	5.13	90	510	5.4	1.4	9.4
ZrO_2 + CaO + CeO_2						
Mixed powders	4.87	83	500	5.2	1.3	10.5
GSP	5.57	95	530	6	1.8	7.9
ZrO_2 + Y_2O_3						
Coprecipitation	5.45	91	490	5.4	1.4	9.7
GSP	5.71	96	500	6.2	1.8	8.7
ZrO_2 + Y_2O_3 + CeO_2						
Coprecipitation	5.69	94	520	6.8	2	8.1
GSP	5.45	90	510	5.6	1.5	8.9

Table 3
Solubility tests (results in wt%)

Type of inert matrix (contents in wt%)	Type of sample	Type of test									
		Leaching in simulated rain water (pH = 3.65)					Leaching in simulated rain water + Na_2CO_3 (pH = 8.00)	Treatement with HNO_3 – 8M			Treatement with concentrated $HN0_3$ + HF after HNO_3 – 8M
		Open vessel room P, T	Closed mW heated (P = 2.5 MPa, T = 493 K)			Open vessel room P, T after mW	Open vessel room P, T	Open vessel room P, T = 383 K	Closed mW heated P = 1.64 MPa T = 493 K		Closed mW heated not controlled P, T (max P = 11 MPa)
		8 months	I (1 h)	II (1 h)	III (1 h)	4 months	8 months	1 h	I (1 h)	II (1 h)	$t = 20'$ mW_{max} = 600 W
Inert matrix type A	Microgranules calcinated at 973 K	0.06 [a]					0.09 [a]	23			67
ZrO_2 (Y_2O_3 16%) = 52.7%	Microgranules sintered at 1823 K	0.004					0.0004 [a]	0.009	0.075	0.005	43
Al_2O_3 = 45.4%	Whole pellets	0.0007	0.0014	0.0002	<0.0001	0.00001 [a]	0.0001 [a]	0.002	0.008	0.003	
MgO = 1.9%	Pulverized pellets							0.014			
Inert matrix type A + CeO_2	Microgranules calcinated at 973 K	0.11 [a]					0.18 [a]	19			64
ZrO_2 (Y_2O_3 16%) = 48.9%	Microgranules sintered at 1823 K	0.002					0.0002 [a]	0.003	0.15	0.004	41
Al_2O_3 = 42.2%	Whole pellets	0.0008	0.0006	0.0001	<0.0001	0.00001 [a]	0.0001 [a]	0.0008	0.014	0.002	
MgO = 1.7%	Pulverized pellets							0.008			41
CeO_2 = 7,2%											
Inert matrix type B ZrO_2 = 90.3%	Whole pellets							0.08	0.13	0.12	
CaO = 9.7%											
Inert matrix type B + CeO_2 ZrO_2 = 81%	Whole pellets							0.04	0.09	0.03	
CaO = 8.7%											
CeO_2 = 10.3%											

[a] only Mg solubilized; mW = microwave heating.

of the third sequential test (in progress) are necessary to confirm this assumption.

The partial solubilisation of microgranules calcinated at 973 K, in 8M HNO_3, points out an incomplete forming reaction for this material.

Only in very highly aggressive conditions such as concentrated HNO_3 + HF attack at high temperature and pressure in a microwave reactor, solubilisation of sintered materials is partially achieved. To better evaluate this result it is necessary however to consider the small amount of sample tested, the sophisticated apparatus employed and the concomitant presence of the fluoride ions in solution.

4. Conclusions

A detailed fuel qualification process is required for the inert matrix-thoria fuel concept aimed at commercial LWRs, starting from basic technological assessment up to extensive irradiation testing.

The early tests carried out so far show that simulated fuel pellets can be fabricated by matching basic nuclear grade specifications such as the required geometry, pellet density and microstructure. That is especially evident when using the GSP process, though some process parameters tuning is still necessary.

Results from thermo-physical characterisation at room temperature are consistent with the literature data. From leaching and dissolution tests it clearly emerges that the inert matrix material displays a very high chemical stability, which represents a strong advantage against diversion purposes and for a safer disposal of the spent inert matrix fuel. The dissolution resistance is not ensured, however, in case of highly aggressive, out of standard technique, nitric acid plus hydrofluoric acid mixture. Awaited observations from the still under-way IID testing on stabilised zirconia, are important to confirm the choice of this material as one of the best candidate inert matrix materials, whose strong ion irradiation damage resistance features have already been referred by other authors [25–27].

Additional fabrication and characterisation testing will also deal with thoria introduction, in view of starting the design and fabrication of the first irradiation experiment expected in the Halden HWBR.

References

[1] C. Lombardi, A. Mazzola, M. Ricotti, Analysis of a Pu–Th Fuel Cycle for the Reduction of the Plutonium Stockpiles, In: Proceedings of ICONE-5: Fifth International Conference on Nuclear Engineering, Nice, France, 26–30 May 1997.

[2] F. Vettraino, C. Lombardi, A. Mazzola, E. Marmo, G. Magnani, G. Zappa, Inert Matrix Fuels for Plutonium Disposition in PWRs, In: Proceedings of ICONE-6 Sixth International Conference on Nuclear Engineering, San Diego, CA, USA, 10–15 May 1998.

[3] F. Vettraino, C. Lombardi, E. Padovani, M.E. Ricotti, A. Mazzola, Innovative U-free Fuels for Weapons Plutonium Disposition in Current LWRs, In: Proceedings of Forum of the UNESCO International School for Peace on Nuclear Disarmament, Safe Disposal of Nuclear Materials or New Weapons Developments?, Villa Erba, Cernobbio, Como, Italy, 2–4 July 1998, UNESCO, in press.

[4] IAEA-TECDOC-941, Recycling of Pu and U in Water Reactor Fuel, May 1997.

[5] AEN/NEA, Management of Separated Plutonium, OECD, 1997.

[6] H. Akie, T. Muromura, H. Takano, S. Matsuura, Nucl. Techn. 107 (1994) 182.

[7] C. Degueldre, J.M. Paratte, Nucl. Techn. 123 (1998) 21.

[8] C. Rubbia, S. Buono, E. Gonzalez, Y. Kadi, J. Rubio, A realistic Plutonium Elimination Scheme with Fast Energy Amplifiers and Th–Pu Fuel, CERN/AT/95–53(ET), December 1995.

[9] IAEA-TECDOC-985, Accelerator Driven Systems: Energy Generation and Transmutation of Nuclear Waste, Status Report, November 1997.

[10] C. Lombardi, A. Mazzola, E. Padovani, M.E. Ricotti, these Proceedings, p. 181.

[11] F. Vettraino, Preleminary Specifications of Inert Matrix Fuel for Plutonium Burning in LWRs, ENEA report no ERG/FISS/GT-FBB-0001 and ERG/FISS/GT-FBB-0002, 1996.

[12] G. Brambilla, P. Gerontopulos, D. Neri, Energia Nucleare 17 (4) (1970) 217.

[13] T.M.G. La Torretta, G. Magnani, Proceedings of Ninth Cimtec, Florence, Italy, 14–19 June 1998.

[14] M.A.C.G. Van Der Graaf, A.J. Burggraaf, Wet-chemical preparation of zirconia powders: their microstucture and behavior, in: N. Clausen, M. Ruhle, A. Heuer (Eds.), Science and Technology of Zirconia II, The American Ceramic Society, Columbus, Ohio, 1984.

[15] M. Beghi, C.E. Bottani, Appl. Phys. 23 (1980) 57.

[16] M. Beghi, M. Berra, G. Caglioti, A. Fazzi, Mater. Construct. 19 (1986) 65.

[17] L.D. Landau, E.M. Lifshitz, Theory of Elasticity, Pergamon, Oxford, 1970.

[18] D.C. Wallace, Thermodynamics of Crystals, Wiley, New York, 1972.

[19] G. Caglioti, Proceedings of LXXXII International School of Physics 'E Fermi', Varenna, Italy, 30 June–10 July 1981, North Holland, Amsterdam, 1982.

[20] L. Luzzi, A new method for measuring thermal conductivity, in: Proceedings of Third Workshop on Inert Matrix Fuel, Bologna, Italy, 20–21 November 20–21 1997, ENEA-Bologna, April 1998.

[21] M.G. Beghi, L. Luzzi, Proceedings of the 24th International Thermal Conductivity Conference and 12th International Thermal Expansion Symposium, Pittsburgh, PA, USA, 26 October 1997, Technomic, Lancaster, 1998.

[22] M.G. Beghi, L. Luzzi, J. Phys.: Measurement Sci. Technol., to be published.

[23] J.G. Hust, A.B. Lankford, Update of Thermal Conductivity and Electrical Resistivity of Electrolytic Iron, Tung-

sten, and Stainless Steel, NBS Special Publication 260-90, 1984.
[24] NIST Certified Reference Materials 1461, 8420, 738, 736L1, 781D2, 5, National Institute of Science and Technology, Gaithersburg, MD, USA.
[25] W.J. Weber, R.C. Ewing, C.R.A. Catlow, T. Diaz de la Rubia, L.W. Hobbs, C. Kinoshita, Hj. Matzke, A.T. Motta, M. Nastasi, E.H.K. Salje, E.R. Vance, S.J. Zinkle, J. Mater. Res. 13 (1998) 1434.
[26] N. Yu, K.E. Sickafus, P. Kodali, M. Nastasi, J. Nucl. Mater. 244 (1997) 266.
[27] E.L. Fleischer, M.G. Norton, M.A. Zaleski, W. Hertl, C.B. Carter, J.W. Mayer, J. Mater. Res. 6 (1991) 1905.